

1 **A Comparison of Shortwave Reflectance Over the**  
2 **East Antarctic Plateau Observed by CERES to that**  
3 **Estimated From Surface Reflectance Observations**

Stephen R. Hudson

4 Norwegian Polar Institute, Tromsø, Norway

Stephen G. Warren

5 Department of Atmospheric Sciences, University of Washington, Seattle,

6 Washington, USA

Seiji Kato

7 Science directorate, NASA Langley Research Center, Hampton, Virginia,

8 USA

9 Submitted to *JGR - Atmospheres* 10 June 2009

---

S. R. Hudson, Norwegian Polar Institute, Polar Environmental Centre, N-9296 Tromsø, Norway. (hudson@npolar.no)

S. G. Warren, Department of Atmospheric Sciences, University of Washington, Box 351640, Seattle, WA 98195-1640, USA. (sgw@atmos.washington.edu)

S. Kato, Science directorate, NASA Langley Research Center, Mail Stop 420, Hampton, VA 23681-2199, USA. (s.kato@larc.nasa.gov)

**Abstract.**

Spectral albedo and bidirectional reflectance of snow were measured at Dome C on the East Antarctic Plateau, for wavelengths 350–2400 nm and solar zenith angles 52°–87°. A parameterization of bidirectional reflectance, based on those measurements, is used as the lower boundary condition in the atmospheric radiation model SBDART to calculate radiance and flux at the top of the atmosphere (TOA). The model’s atmospheric profile is based on radiosoundings at Dome C and ozonesoundings at the South Pole. Computed TOA radiances are integrated over wavelength for comparison with the CERES short-wave channel. CERES radiance observations and flux estimates from four clear days in January 2004 and January 2005 from within 200 km of Dome C are compared with the TOA radiances and fluxes computed for the same solar zenith angle and viewing geometry, providing about 20,000 comparisons. The measured radiance and flux are lower than the computed values. The median difference is 3.8–4.6% for CERES on Terra, and 5.6–7.3% on Aqua. Sources of uncertainty in the model and observations are examined in detail, and suggest that the measured values should actually be higher than the computed values, by  $2\% \pm 4\%$ . The source of the discrepancy cannot be identified here; however, the modelled values do agree with observations from another satellite instrument (MISR), suggesting that the CERES calibration must be considered a possible source of the discrepancy.

## 1. Introduction

31 In a companion paper [*Hudson et al.*, 2009], we examined uncertainties in angular  
32 distribution models (ADMs) used by the Clouds and the Earth's Radiant Energy Sys-  
33 tem (CERES) experiment for converting observed top-of-atmosphere (TOA) radiances to  
34 hemispheric fluxes over permanently snow-covered regions with clear skies. That was done  
35 by comparing the angular distribution of reflected radiance from the ADMs with that from  
36 a radiative transfer model that used snow surface reflectance and atmospheric conditions  
37 based on measurements at Dome C Station on the East Antarctic Plateau (75° S, 123° E,  
38 3200 m). The details of the model are given in Section 2 of *Hudson et al.* [2009], and the  
39 terminology used to describe directional reflectance is explained in Section 1 of *Hudson*  
40 *et al.* [2009].

41 In this paper we run the same model and compare the magnitude of reflected radi-  
42 ances and fluxes observed by CERES to those obtained from a model applied to surface  
43 observations, so as to compare the calibration of the CERES shortwave instruments and  
44 the model. The model was run as in the companion paper, but at 1-degree intervals of  
45 solar zenith angle ( $\theta_o$ ), with output saved at 2-degree intervals of viewing zenith angle  
46 ( $\theta_v$ ) and 3.75-degree intervals of relative azimuth ( $\phi$ ). The modelled radiance or flux at  
47 the solar zenith angle and viewing geometry of CERES observations is then determined  
48 by interpolating the stored values in solar zenith, viewing zenith, and relative azimuth  
49 angles.

50 The Antarctic Plateau is a large, spatially and temporally homogeneous region of  
51 the planet, with a clean, dry, optically thin atmosphere, making it an appealing area for

52 use in satellite-model comparisons. The region has previously been used as a calibration  
53 target for AVHRR [*Loeb, 1997; Masonis and Warren, 2001*].

54 We begin by comparing the ADM albedos, which are representative of the mean  
55 albedo observed by CERES over all permanently snow-covered regions, to the model's  
56 albedo. Following that we examine the differences in more detail by comparing approxi-  
57 mately 20,000 CERES radiances and fluxes observed on clear days in the region around  
58 Dome C with the modelled radiance and flux at the same solar and viewing angles. We  
59 then examine sources of uncertainty and try to explain the differences we find between  
60 the model and observations.

## 2. Comparison of Modelled and ADM Albedo

61 Figure 1 compares the albedo from the CERES permanent snow ADMs [*Kato and*  
62 *Loeb, 2005*] with that from the model. *Kato and Loeb* [2005] developed two clear-sky  
63 permanent-snow ADMs, differentiated by the surfaces' nadir brightness; albedos from  
64 both ADMs are shown in Figure 1. The different shapes of the model and ADM curves  
65 at large solar zenith angles is due to the different geometry of the atmosphere and model.  
66 At these large solar zenith angles, a significant fraction of the reflected light at the TOA  
67 did not enter the atmosphere above the observation location, but was scattered through  
68 the atmosphere to that location; the plane-parallel model used here does not account for  
69 this scattered light, which entered the atmosphere at a smaller zenith angle as a result  
70 of the Earth's curvature. The model also overestimates the atmospheric path length,  
71 compared to the real path length through the spherical atmosphere, therefore causing too  
72 much absorption at large solar zenith angles. At smaller solar zenith angles there is a  
73 general trend of slightly increasing albedo with solar zenith angle. This trend is caused

74 by the increase in surface albedo with increase in solar zenith angle, especially at near-  
75 infrared wavelengths. At  $\theta_0 < 80^\circ$ , the model albedos are higher than the ADM albedos  
76 by 0.05—0.08.

77 Dome C is one of the higher, drier permanent snow regions, with only 0.7 mm of  
78 precipitable water in the model summertime atmosphere used here. To see if this lack of  
79 water vapor could account for the albedo difference seen here, the model was run with  
80 a solar zenith angle of  $75^\circ$ , using the subarctic winter atmosphere [McClatchey *et al.*,  
81 1972], which contains 4 mm of precipitable water. Using this atmosphere reduced the  
82 model albedo from 0.729 to 0.661, in line with the ADM albedos. Thus the albedo  
83 difference could be explained if most of the permanent snow seen by CERES were under  
84 an atmosphere with large amounts of water vapor. However, varying water-vapor amount  
85 is not likely to explain much of the difference, for the following reasons. First, most  
86 of Antarctica has less precipitable water than the subarctic winter atmosphere, even in  
87 the warmest month (January), according to the NCEP/NCAR Reanalysis. Second, the  
88 subarctic winter atmosphere has a column ozone amount of 486 Dobson units, about  
89 75% more than the January Antarctic atmosphere, according to NOAA-GMD ozonesonde  
90 data and to Global Ozone Monitoring Experiment data [Burrows *et al.*, 1999]. Third,  
91 Antarctica has 8 times the area of Greenland, so most of the permanent snow used by  
92 CERES to develop ADMs would have had water-vapor amounts far lower than Arctic  
93 values. Finally, a separate comparison was made with non-operational CERES ADMs  
94 developed with data from only the region around Dome C, and it showed similar differences  
95 between the model and ADM albedos.

### 3. Comparison with Individual Observations

96 To try to assess the accuracy of the model output and of CERES radiance and  
97 flux data from observations over the area around Dome C, modelled radiances and fluxes  
98 are compared with CERES observations from this region. CERES observations from all  
99 four polar-orbiting instruments were used, and all were taken from Edition 2B-rev1 SSF  
100 data [Matthews *et al.*, 2005]. CERES data with surface footprints lying within 200 km  
101 of Dome C were gathered from 3 days in January 2004 and 1 day in January 2005,  
102 during times when our visual observations from the surface indicate that skies were free  
103 of clouds and boundary-layer ice crystals at Dome C Station for at least 6 hours (data are  
104 from 9 overpasses on 13 January 2004 spread between 0600 and 2400 local standard time  
105 (UTC+8), 16 overpasses spread between 1700 on 18 January and 1800 on 19 January  
106 2004, 8 overpasses spread between 1900 on 21 January and 0900 on 22 January 2004, and  
107 3 overpasses around 0900, 1100, and 2200 on 28 January 2005). This provided 23,257  
108 radiance observations that were used by CERES to determine fluxes (with  $\theta_o < 86.5^\circ$  and  
109  $\theta_v < 70.0^\circ$ ). Of these observations, 20,700 were identified by CERES as having clear skies,  
110 and only this subset was used in the comparison.

111 The relative difference between each CERES radiance observation and the modelled  
112 radiance at the same solar zenith, viewing zenith, and relative azimuth angles was cal-  
113 culated, along with the relative difference between each CERES flux calculation and the  
114 modelled flux at the same solar zenith angle. The results are summarized, as functions  
115 of solar or viewing zenith angle, in Figures 2 to 5. In each of these figures, the data are  
116 grouped into 2-degree bins in  $\theta_o$  or 5-degree bins in  $\theta_v$ , and are summarized with box plots  
117 that show, for each bin, the median difference, the upper and lower quartiles, the 5<sup>th</sup> and

118 95<sup>th</sup> percentiles, and the range of differences. The figures also show the number of obser-  
119 vations in each bin, which varies significantly in Figures 2 and 3 because the satellites'  
120 orbits cause them to pass near Dome C most often in mid-morning and late-evening, local  
121 time.

122 The general pattern seen in these figures is that the CERES radiances and fluxes  
123 are smaller than the modelled values, with a median difference of about 5%. Comparing  
124 Figure 2 with 3, or Figure 4 with 5, we see that the outlying data with large negative dif-  
125 ferences in the radiance plots have the magnitude of their differences significantly reduced  
126 in the flux plots. This is due to differences between the model and CERES anisotropic  
127 reflectance patterns (see the companion paper [*Hudson et al.*, 2009]), which can cause the  
128 relative difference in the flux estimate to differ from the relative difference in the radiance  
129 measurement.

130 Those large differences represent a small fraction of the data; fewer than 1.1% of  
131 the radiance observations differ from the model by more than 25%, whereas 80% of the  
132 observations differ from the model by between 0 and -10%, with a median of -4.7%.  
133 The only observations in which the CERES radiances or fluxes are systematically larger  
134 than the modelled values are those made when the solar zenith angle was very large, again  
135 a result of the plane-parallel geometry of the model, as described in Section 2. Taking  
136 observations from the four polar-orbiting CERES instruments separately (there are two  
137 CERES instruments on the Terra satellite, called FM1 and FM2, and two on the Aqua  
138 satellite, called FM3 and FM4), the median differences are: -4.1% for FM1, -4.2% for  
139 FM2, -5.6% for FM3, and -5.2% for FM4.

140 Some scatter is to be expected in comparisons between CERES observations and  
141 the model since the model has an atmosphere and snow surface that are representative of  
142 average summer conditions at Dome C, but the CERES observations see both spatial and  
143 temporal variability. However, the consistent bias seen in the Figures 2 to 5 suggests that  
144 the model overestimates the reflectance, or that CERES underestimates the reflectance, or  
145 both. To try to see if the model is overestimating the reflectance for some reason, modelled  
146 reflected radiances at four wavelengths were compared with the radiances observed within  
147 50 km of Dome C by the Multiangle Imaging SpectroRadiometer [MISR; *Diner et al.*, 1998]  
148 during five overpasses of Dome C. MISR observes the light reflected from a location at  
149 nine viewing angles within 10 minutes, allowing comparisons to be made over a variety  
150 of viewing angles. Its four spectral channels lie in the blue, green, red, and near-infrared  
151 regions.

152 A representative example of these comparisons, using the 672-nm (red) channel, is  
153 shown in Figure 6. This figure shows the distribution of observed bidirectional reflectance  
154 factors (BRF, equal to  $\pi$  times the reflected radiance, divided by the incident flux) and  
155 the corresponding modelled BRF. In these comparisons, the shape of the modelled re-  
156 flectance versus viewing zenith angle compares well with the MISR observations. Of the  
157 180 individual comparisons we made (5 overpasses with 9 cameras, each with 4 channels),  
158 the modelled reflectance was above the MISR-observed range of reflectance only 5 times;  
159 it was in the upper quartile of the range 8 times, within the interquartile range 27 times,  
160 in the lower quartile 32 times, and below the range of observed values 108 times. The  
161 median radiance difference ( $(\text{MISR} - \text{Model})/\text{Model}$ ) of all observations within 50 km of  
162 Dome C from the 5 overpasses is +3.5%, and the interquartile range is +1.2% to +5.6%.

163 Thus, whereas the model radiance exceeds the CERES radiance, it is usually lower than  
164 the MISR radiance.

165 The absolute uncertainty in MISR radiances is estimated to be within 4% (1 standard  
166 deviation level of confidence) for bright, uniform targets [*MISR Science Team*, 2004;  
167 *Bruegge et al.*, 2002]. That large uncertainty means that, this comparison cannot be  
168 taken as proof that CERES is underreporting the reflected radiance near Dome C. We  
169 must now examine known uncertainties in the model and in the CERES observations  
170 to try to see what can be said about the differences between the CERES-observed and  
171 modelled radiances.

#### 4. Uncertainties

172 In this section we examine uncertainties in both the model and the observations to  
173 try to determine if the differences presented above are statistically significant. Potential  
174 sources of error in the modelled reflectance fall into four main categories: (1) the albedo  
175 specified at the lower surface may be biased or affected by random variability; (2) the  
176 parameterization of the anisotropic reflectance factor used for the lower boundary in  
177 the model may be in error; (3) the atmospheric model may incorrectly handle gaseous  
178 absorption, or atmospheric variability may affect the results; and (4) the solar spectrum  
179 used in the model may differ from what was incident at the time of the observations. In  
180 the sections below we consider each of these sources in detail, and then try to estimate  
181 the 95% confidence interval around the expected difference between the CERES-observed  
182 and modelled radiances and fluxes.

## 4.1. Albedo

### 4.1.1. Error in the Albedo Measured at Dome C

The snow-surface albedo measured under a cloud at Dome C and presented by *Hudson et al.* [2006] is used in the parameterization of the anisotropic reflectance factor ( $R$ ), and was also used to determine the best snow grain sizes to use for modelling the spectral albedo as a function of solar zenith angle (see Section 2 of *Hudson et al.* [2009] and Section 4 of *Hudson and Warren* [2007]). There is naturally some uncertainty in this measurement, which is discussed here; however, this uncertainty does not directly affect the model results presented above, but rather affects the uncertainty of the modelled surface albedo and of the parameterization of  $R$ , both of which are discussed below. For this reason, the uncertainties discussed here are not included in the final table of all uncertainties affecting the measurements and model.

The largest source of uncertainty in the albedo measurement is the correction that had to be applied to the raw measurements to account for the shadow of the instrument and observer. Two separate methods used to determine this correction, one geometrical and the other based on consistency in derived grain sizes at different wavelengths, both suggested the raw albedo must be increased by 4% to obtain the actual albedo [*Brandt and Warren*, 2009, Appendix]. The correction factor that was used was 4.2%, but we estimate the uncertainty of the correction is  $\pm 1\%$ . The 4.2% correction results in visible albedos that are 0.006 higher than those measured previously at South Pole and Vostok Stations [*Grenfell et al.*, 1994, Table 6]. (The shadow correction of 4% is considerably larger than that applied by *Grenfell et al.* [1994], but a different instrument was used at Dome C, and 4% was judged appropriate for its geometry).

205 The albedo measurement consists of a ratio of two flux spectra, both made with  
206 the same instrument and cosine collector, so the calibration of the instrument does not  
207 affect the resulting albedo. On the evening when the albedo was measured there was a  
208 thick overcast that diffused the solar beam, minimizing errors due to imperfect cosine  
209 response and errors due to tilt of the instrument or surface. The measured albedo was  
210 determined by averaging 10 albedo observations made over a period of about 10 minutes  
211 (6 incident spectra and 5 reflected spectra; 10 albedos were calculated by dividing each  
212 reflected spectrum by the incident spectra measured immediately before and after it).  
213 Some smoothing in wavelength was then done to reduce noise by applying a running  
214 mean. The standard deviation of the 10 individual unsmoothed albedo observations is  
215 between 0.0025 and 0.004 at wavelengths less than 900 nm, and between 0.003 and 0.007  
216 at most wavelengths between 900 and 1700 nm. Smaller signal to noise ratios at longer  
217 wavelengths result in standard deviations between about 0.02 and 0.12. The standard  
218 deviation of the 10 broadband (350 to 2400 nm) albedos is 0.0036 (0.46%). This provides  
219 a good estimate of the uncertainty in the measurement that is not related to the shadowing  
220 correction.

221 The snow surface above which the albedo at Dome C was measured was smoother  
222 than most of the snow around Dome C. Wind-erosion features called sastrugi are respon-  
223 sible for the surface roughness on the Antarctic Plateau; a photograph is shown in Figure  
224 2 of *Hudson et al.* [2006]. The Dome-C region has smaller sastrugi than most of Antarc-  
225 tica because of the light winds that are found there, but accurately measuring the albedo  
226 above even small sastrugi would require being well above the surface, which was not pos-  
227 sible to do without standing on a tower that would dramatically disrupt the field of view.

228 Therefore, an unrepresentatively smooth region of snow was chosen for the measurement.  
229 Taking 10 cm as the typical height of sastrugi at Dome C and 1 m as the typical spacing  
230 between sastrugi tops gives a height-to-width ratio of the sastrugi at Dome C of 0.1 [see  
231 Section 3.1 of *Hudson et al.*, 2006, for a description of the snow surface roughness at  
232 Dome C]. Using this height-to-width ratio with results from Figure 13b of *Warren et al.*  
233 [1998] and with the spectral albedo from Dome C, we estimate that the broadband albedo  
234 over the smooth snow may be up to 0.0065 (0.8%) too high, compared to that for the  
235 rough surface. This is should be viewed as an upper limit for this error since the observed  
236 snow surface was not perfectly smooth and 0.1 is probably an overestimate of the typical  
237 height-to-width ratio.

#### 238 4.1.2. Error in the Modelled Surface Albedo

239 The modelled albedo is used in two ways in this paper: first, the modelled diffuse  
240 albedo is used to provide the necessary input to the parameterization for  $R$  at wavelengths  
241 longer than  $2.4 \mu\text{m}$ , for which we did not measure the albedo; second, the modelled  
242 direct-beam albedo for all incidence angles is used to convert  $R$ , a normalized directional  
243 reflectance, to the bidirectional reflectance factor (BRF).

244 The modelled diffuse albedo is used only for the calculation of  $R$  at wavelengths  
245 longer than  $2.4 \mu\text{m}$ . Errors in this modelled albedo would lead to an incorrect angular  
246 distribution of reflected flux at those long wavelengths, but would not affect the amount  
247 of reflected flux at the surface. Since only about 0.1% of the reflected flux has wavelength  
248 longer than  $2.4 \mu\text{m}$  under a clear sky with  $\theta_o = 60^\circ$ , errors in the modelled diffuse albedo  
249 will not have any significant impact on our results.

250 The modelled direct-beam albedo is more important; it is used to convert the calcu-  
251 lated  $R$  to a BRF, and therefore determines the overall albedo of the surface. This albedo  
252 had to be modelled since accurately observing the direct-beam spectral albedo under all  
253 incidence angles was not possible on the natural snow (the albedo at all incident zenith  
254 angles, even those never obtained by the sun, must be known so that the model can handle  
255 diffuse incidence, and the albedo must be for pure direct-beam incidence, not the natural  
256 mix of direct and diffuse found at the surface).

257 We modelled the albedo in SBDART with no atmosphere and with two snow layers:  
258 a semi-infinite layer of 90- $\mu\text{m}$  grains below a 0.25-mm layer of 40- $\mu\text{m}$  grains. The snow  
259 grains were specified as having the single-scattering albedo of an ice sphere of the given  
260 radius and a Henyey-Greenstein phase function with asymmetry factor of an ice sphere  
261 of the given radius. The Mie calculations were done using the updated ice absorption  
262 coefficients from *Warren et al.* [2006]. *Grenfell et al.* [1994] found that such a two-layer  
263 snow model was better able to match Antarctic albedo measurements since the natural  
264 snow often has small grains at the very surface because they are the last to fall back to  
265 the surface after blowing snow events. The two grain sizes were determined by modelling  
266 the albedo under a thick cloud with the specified grain sizes of the two layers varying from  
267 20 to 120  $\mu\text{m}$ , and finding which combination best matched the observed albedo under a  
268 cloud (by minimizing the root mean squared error [RMSE] over all wavelengths).

269 Errors in the specified grain sizes and in the single-scattering properties of the grains,  
270 as well as uncertainty in the ice absorption spectrum, all combine to create uncertainty  
271 in modelled albedo. Using a different model and different methods, *Brandt and Warren*  
272 [2009] used the same albedo measurement and estimated the snow to have 50- $\mu\text{m}$  grains

273 over 80- $\mu\text{m}$  grains. Comparing modelled clear-sky albedo with  $\theta_o = 60^\circ$  for snow grains  
274 of 30 to 50  $\mu\text{m}$  over snow grains of 80 to 100  $\mu\text{m}$ , indicates an uncertainty in the modelled  
275 albedo due to grain size uncertainty (full range of these modelled albedos) of 0 to  $\pm 0.0023$   
276 in the visible (increasing with wavelength), increasing to  $\pm 0.029$  at 1.3  $\mu\text{m}$ , and to  $\pm 0.045$   
277 at 2.25  $\mu\text{m}$ . The resulting uncertainty in the broadband albedo is  $\pm 0.009$ , which is  $\pm 1.1\%$ .  
278 Since we looked at the full range of the different albedos, we will take this to be a  $2\text{-}\sigma$   
279 uncertainty due to grain size uncertainty.

280 The Henyey-Greenstein phase function was used for modelling the spectral albedo.  
281 This represents a computational convenience, not an attempt to accurately describe the  
282 real phase function. Nevertheless, it is often used in atmospheric radiative transfer mod-  
283 elling and was shown by *Hansen* [1969] to result in accurate albedo calculations for  
284 conservatively-scattering, optically-thick clouds. More recently, *Aoki et al.* [2000] showed  
285 it can be used to accurately model reflectance from snow, with differences between the  
286 spectral albedo modelled with the full Mie phase function and that modelled with the  
287 Henyey-Greenstein phase function of around 0.0015 or less at all wavelengths from 0.35  
288 to 2.5  $\mu\text{m}$  (their Figure 14). If we take an uncertainty in the modelled spectral albedo  
289 due to the choice of phase function of  $\pm 0.0015$ , this gives an uncertainty in the broadband  
290 albedo under clear sky with  $\theta_o = 60^\circ$  of  $\pm 0.2\%$ .

291 There remains some uncertainty regarding the complex index of refraction of pure  
292 ice, which is used as an input to the Mie calculations that determine the single-scattering  
293 properties of the snow grains. *Warren and Brandt* [2008] recently published an updated  
294 compilation of the complex index of refraction of ice. For our model, the most important  
295 difference between the new values and the old standard [*Warren, 1984*] is reduced absorp-

tion in the ultraviolet and shortwave visible wavelengths, based on the results of *Warren et al.* [2006]. To estimate the uncertainty in the modelled albedo due to uncertainty in the ice optical properties, we compare the albedo modelled with the newly-compiled values to those modelled with the older compilation. Under clear sky with  $\theta_o = 60^\circ$ , spectral albedo differs by up to 0.04; the broadband albedo is 0.3% higher with the newly-compiled values. Based on this we take an uncertainty in modelled albedo of  $\pm 0.3\%$ .

Combining the three sources of uncertainty gives an overall uncertainty in the modelled radiance and flux due to uncertainty in the calculated albedo of  $\pm\sqrt{1.1^2 + 0.2^2 + 0.3^2} = \pm 1.2\%$ . We consider this to be a good estimate of the  $2\text{-}\sigma$  uncertainty of the broadband albedo at the surface under the clear, Dome-C model atmosphere. This error is taken to be a bias of unknown sign, since increasing the number of observations used in the comparison will not reduce the effect of this uncertainty. We can also include the bias due to sastrugi, as discussed in the previous section, in which the albedo of the modelled flat surface is potentially up to 0.8% higher than that of the natural snow surface.

### 4.1.3. Spatial and Temporal Albedo Variability

Previous studies of broadband albedo on the East Antarctic Plateau have shown values in December and January varying between about 0.8 and 0.87, without much variability between South Pole, Dome C, Vostok, and Plateau Stations [*Grenfell et al.*, 1994; *Pirazzini*, 2004; *Kuhn et al.*, 1977]. The lack of any systematic variability in the albedo at the different stations indicates that we need to concern ourselves mostly with temporal variability. Most of the variability that is reported is due to variability of solar

318 zenith angle and cloudiness. Our modelled spectral albedos result in broadband albedos  
319 that vary from 0.809 at  $\theta_o = 50^\circ$  to 0.887 at  $\theta_o = 89^\circ$ .

320 From the data presented for December 1966 and January 1967 in Figure 7 of *Kuhn*  
321 *et al.* [1977], we calculated a standard deviation of daily-mean summertime albedo at  
322 Plateau station of 0.018, which is 2.2% of the mean of the daily albedos (0.825). Data  
323 obtained from the NOAA observatory at South Pole for January 2007, 2008, and 2009  
324 showed a clearly increasing albedo from year to year (the January-mean albedo was 0.851,  
325 0.874, and 0.899 in 2007, 2008, and 2009), which is almost certainly a spurious trend.  
326 Therefore, the standard deviation of the departure of the daily-mean albedo from the  
327 monthly-mean albedo for that particular January was calculated for this 3-month dataset,  
328 and also happened to be 0.018. Some of the variability at both stations is due to day-  
329 to-day changes in cloudiness and solar zenith angle, so we assume that a little more than  
330 half of the variability is due to real temporal changes in the snow, and estimate that the  
331  $2\text{-}\sigma$  uncertainty in an individual comparison between our model results and a CERES  
332 observation, due to spatial and temporal albedo variability, is around  $\pm 2.5\%$ . Despite the  
333 fact that large-scale spatial albedo variability is very small (i.e. in the mean albedo from  
334 one station to another), temporal variability will show up as small-scale spatial albedo  
335 variability since not all areas experience the same changes simultaneously. Assuming  
336 we can consider the four days from which observations were used in the comparisons as  
337 independent samples, then this uncertainty is reduced to  $\pm 2.5\% / \sqrt{4} = \pm 1.25\%$  for the  
338 overall comparison.

## 4.2. Anisotropic Reflectance Factor

339 The sections above discuss the uncertainty in the model's specification of the re-  
340 flected surface flux, but the modelled radiances are also affected by the uncertainty in the  
341 model's specification of the angular distribution of this reflected flux. This distribution is  
342 taken from the parameterization for the surface anisotropic reflectance factor presented  
343 by *Hudson et al.* [2006]. Table 1 of *Hudson et al.* [2006] gives the RMSE of the parame-  
344 terized values of  $R$  for different ranges of  $\lambda$ ,  $\theta_o$ , and  $\theta_v$ . Ignoring the contribution of error  
345 in individual measurements to the RMSE, we take these values to be representative of the  
346  $1-\sigma$  uncertainty due to the parameterization.

347 Around 80% of the reflected energy at the TOA is at  $\lambda < 950$  nm, and most of the  
348 viewing zenith angles in the CERES-model comparisons were  $52.5^\circ$  or less, so we use the  
349 RMSE for the parameterization for  $350 \leq \lambda \leq 950$  nm, calculated for  $\theta_v \leq 52.5^\circ$ , which is  
350 1.9% for  $\theta_o < 75^\circ$  and 3.0% for  $\theta_o > 70^\circ$ . Averaging these two values, we estimate the  $1-\sigma$   
351 uncertainty due to the parameterization is  $\pm 2.5\%$ . Much of this uncertainty represents  
352 variability in  $R$ , but some is also due to errors in the parameterization. Since we cannot  
353 accurately separate the two contributions, we assume only 2, rather than 4, independent  
354 samples, reducing the  $2-\sigma$  uncertainty estimate from  $\pm 5\%$  to  $\pm 3.5\%$ .

355 As described by *Hudson et al.* [2009], the surface  $R$  at all wavelengths less than  
356 800 nm was assumed to be equal to that at  $\lambda = 800$  nm. This was done because the mea-  
357 surements, and therefore the parameterizations, of  $R$  at shorter wavelengths are affected  
358 by diffuse incidence from Rayleigh scattering, and because the direct-beam  $R$  correlates  
359 well with albedo, which doesn't change much between 800 and 300 nm. The accuracy of  
360 this assumption was tested in Section 5.3 of *Hudson et al.* [2006], where their Figure 15

361 shows the relative error caused by assuming  $R$  at 375 nm was equal to  $R$  at 900 nm. This  
362 shows that, for most  $\theta_v < 70^\circ$ , the error is within  $\pm 3\%$ . This represented an extreme  
363 test for this assumption (starting with 900, rather than 800 nm, and comparing with  
364 the wavelength with the highest albedo), and only 65% to 70% of the reflected energy  
365 is affected by this assumption, so we estimate the  $2\text{-}\sigma$  uncertainty associated with this  
366 assumption to be  $\pm 2.5\%$ .

367 Combining these two uncertainties related to the parameterization of  $R$  gives an  
368 overall uncertainty for an individual radiance comparison of  $\pm\sqrt{3.5^2 + 2.5^2} = \pm 4.3\%$ .  
369 The sign and magnitude of the error in the parameterized  $R$  varies with viewing and solar  
370 geometry. Therefore, when we combine all of our comparisons from different solar and  
371 viewing zenith angles, the effect of this uncertainty is reduced. We used observations made  
372 with various combinations of  $\theta_v$  from  $0^\circ$  to  $70^\circ$ , and  $\theta_o$  from  $54^\circ$  to  $86^\circ$ ; we assume that  
373 this gives us at least 10 independent samples in the  $\theta_v\text{-}\theta_o$  space, reducing this uncertainty  
374 to  $\pm 4.3/\sqrt{10} = \pm 1.4\%$ . This uncertainty affects only the radiance comparisons, not the  
375 flux comparisons.

### 4.3. Atmospheric Model

#### 4.3.1. Error in Modelled Gaseous Absorption

377 Here we attempt to assess the uncertainty in the model results due to errors in the  
378 specification of gaseous absorption in the radiative transfer model. The model we used,  
379 SBDART, was one of the models entered into an intercomparison study presented by  
380 *Halthore et al.* [2005], which examined the performance of 16 shortwave radiative transfer  
381 models in various case studies, including one with a clear, aerosol-free, subarctic winter  
382 atmosphere and a solar zenith angle of  $75^\circ$ . From the results of *Halthore et al.* [2005, in the

383 Auxiliary Materials file 2004JD005293-case1.txt], we see that SBDART and the related  
384 model SBMOD (which uses the HITRAN, rather than LOWTRAN-7, absorption data)  
385 both calculated more atmospheric absorption than most of the other models (SBDART  
386 calculated that the atmosphere absorbs 19.9% of the flux incident at the TOA, while the  
387 mean and standard deviation from all 15 models were 18.9% and 0.9%). This increased  
388 absorption resulted from higher near-infrared absorption in SBDART than in the other  
389 models.

390 If the model produces too much atmospheric absorption at wavelengths where the  
391 surface albedo is low, it will have less of an effect on the TOA reflectance than if it does so  
392 where the albedo is high, since much of the extra energy absorbed by the atmosphere would  
393 have been absorbed by the surface anyway. In the near-infrared band used by *Halthore*  
394 *et al.* [2005] (0.7–5.0  $\mu\text{m}$ ), about half of the atmospheric absorption in our model occurs at  
395 wavelengths where the snow albedo is less than 0.5. This distribution of the atmospheric  
396 absorption will reduce the overall effect on the TOA reflectance results, compared to what  
397 it would be if the (presumably spurious) absorption occurred at visible wavelengths, where  
398 the snow is very bright. Further minimizing the importance of this potential model error  
399 is the fact that our Dome-C model atmosphere has about one sixth as much water vapor  
400 as the subarctic winter atmosphere, leading to a reduction in the atmospheric absorption  
401 in this near-infrared band of about 45%.

402 *Halthore et al.* [2005] reported a standard deviation of broadband atmospheric ab-  
403 sorptance, among the models they tested, of 4.7% of the mean absorptance in all models.  
404 With a solar zenith angle of  $70^\circ$ , 4.7% of the atmospheric absorptance in our model is  
405  $3 \text{ W m}^{-2}$ , or 0.87% of the TOA reflected flux. We reduce this uncertainty by 25% to

406 account for the fact that surface absorption will partially compensate for errors in atmo-  
407 spheric absorption, and then double it to get a  $2\text{-}\sigma$  uncertainty of  $\pm 1.3\%$  due to uncertainty  
408 in gaseous absorption in the model. We could choose to use the results of *Halthore et al.*  
409 [2005] to specify a negative bias in the modelled reflected flux, but since it is not clear  
410 which, if any, of the tested models is right, we choose to define this as an uncertainty of  
411 unknown sign.

### 412 4.3.2. Spatial and Temporal Variability of the Atmosphere

413 The model was run with an atmosphere that is representative of the mean atmo-  
414 spheric conditions over Dome C in summer. Here we attempt to assess the uncertainty  
415 due to atmospheric variability. All of the CERES observations considered were made  
416 within 200 km of Dome C, where the surface elevation does not change much, so we do  
417 not need to consider the full range of atmospheric variability over permanent snow, as we  
418 did in the companion paper. Instead, we ran the model in four modified configurations:  
419 1) with twice as much precipitable water, 2) with half as much precipitable water, 3) with  
420 an increase in total ozone concentration of 20 Dobson Units (DU), and 4) with a decrease  
421 in total ozone concentration of 20 DU. Other than the stated changes, the model was  
422 configured exactly as in the standard runs, with a solar zenith angle of  $70^\circ$ . The choice of  
423 ozone variability was made based on daily observations of ozone concentration over Dome  
424 C made in January 2004 and 2005 by the Total Ozone Mapping Spectrometer (TOMS),  
425 which show a mean value of 281 DU, and a standard deviation of 9 DU.

426 Halving or doubling the precipitable water caused an increase of  $1.1\%$  or a decrease  
427 of  $1.4\%$  in the TOA reflected flux, and changed the TOA reflected radiances at the viewing  
428 angles used by CERES by up to  $\pm 1.8\%$ . Changing the total column ozone amount by

429  $\pm 20$  DU changed the TOA reflected flux by  $\pm 0.3\%$ , and changed the TOA reflected  
430 radiances at the CERES viewing zenith angles by up to  $\pm 0.35\%$ . Based on these results,  
431 we take the uncertainty in individual comparisons due to atmospheric variability to be  
432  $\pm \sqrt{1.8^2 + 0.4^2} = \pm 1.8\%$ . Again assuming 4 independent samples, this is reduced to  
433  $\pm 0.9\%$ .

## 4.4. Solar Spectrum

### 4.4.1. Incident Broadband Flux

435 The LOWTRAN-7 solar spectrum was used in our model, and no correction was  
436 made for variations in the Earth-Sun distance. The result was an incident flux at the top  
437 of the atmosphere of  $1372.3 \text{ W m}^{-2}$  in the model. Newer estimates of the solar constant  
438 are closer to  $1366 \text{ W m}^{-2}$  with variability on the order of  $\pm 0.15\%$  [Fröhlich, 2006].

439 The CERES data used in this paper were collected in January, when the Earth-Sun  
440 distance is, on average, 0.9839 times the annual-mean Earth-Sun distance, which results in  
441 an incident flux at the TOA that is  $0.9839^{-2}$  times the solar constant, i.e.  $1411 \text{ W m}^{-2}$  if  
442 the real solar constant is  $1366 \text{ W m}^{-2}$ . Therefore, the TOA incident flux in the model was  
443 2.7% lower than it was in reality. This means our modelled reflected fluxes and radiances  
444 have a negative bias of about  $2.7\% \pm 0.15\%$ . This bias affects only the direct comparisons  
445 of radiance or flux, as shown in Figures 2 to 5, not comparisons of quantities that are  
446 normalized by the incident flux, such as albedo or BRF.

### 4.4.2. Spectral Distribution of Solar Flux

448 In addition to the total solar flux incident at the top of the atmosphere, the spectral  
449 distribution of the incident energy is also important for determining the reflected radiance  
450 and flux. We ran the model using a solar spectrum measured on 15 January 2005 by

451 the Solar Radiation and Climate Experiment [SORCE; *Rottman, 2005*]. The SORCE  
452 spectrum extends only to  $\lambda = 2.4 \mu\text{m}$ , so beyond this, the spectrum was assumed to be  
453 that of a blackbody with a temperature equal to the blackbody temperature determined  
454 from the SORCE flux at  $\lambda = 2.4 \mu\text{m}$ . At wavelengths between 0.4 and 2  $\mu\text{m}$ , the SORCE  
455 and LOWTRAN spectral fluxes differ by up to  $\pm 10\%$ , while at shorter wavelengths the  
456 differences are up to  $\pm 45\%$ . At longer wavelengths the SORCE fluxes are about 10%  
457  $\pm 10\%$  larger than the LOWTRAN fluxes. The main effect of the switch in incident  
458 spectra is to reduce the incident flux at  $\lambda < 0.9 \mu\text{m}$ , and to increase it between 1.5 and  
459 4  $\mu\text{m}$ .

460 The shift of energy to longer wavelengths resulted in a reduction of TOA albedo  
461 with  $\theta_o = 60^\circ$  of 0.0052, or 0.72%. After adjusting for the small difference in broadband  
462 flux between the two incident spectra, the reflected TOA radiances were reduced by 0.54  
463 to 0.77%. Based on this test, we estimate that the uncertainty in the model results due  
464 to uncertainty in the spectral distribution of solar energy is about  $\pm 1\%$ .

#### 4.5. CERES Instrument and Processing

465 *Dong et al. [2008]* estimate the 2- $\sigma$  uncertainty in CERES-observed shortwave broad-  
466 band radiance to be  $\pm 2\%$ , with negligible random noise. An additional source of uncer-  
467 tainty in the CERES measurements comes from the “unfiltering” process, in which a  
468 model-derived regression analysis is used to estimate the total amount of reflected solar  
469 radiance, at all wavelengths, from the observed upwelling radiance in the CERES short-  
470 wave channel. This unfiltering process makes use of the CERES observations from the  
471 shortwave and longwave-window channels, and it removes the spectral filtering of the in-  
472 strument (i.e. accounts for the spectral response function), and eliminates the component

473 of the upwelling radiance that is observed by the instrument that is from thermal emis-  
474 sion. *Loeb et al.* [2001] developed the unfiltering method, and estimate the  $2\text{-}\sigma$  uncertainty  
475 associated with it to be  $\pm 0.8\%$ . Therefore, the overall uncertainty in the CERES radiance  
476 observations is  $\pm 2.2\%$ .

477 A third source of uncertainty must be considered for the CERES fluxes: that associ-  
478 ated with the radiance to flux conversion using the CERES angular distribution models.  
479 Based on the results presented in our companion paper [*Hudson et al.*, 2009], we estimate  
480 this to be  $\pm 4\%$  for individual flux comparisons. As in Section 4.2, this error varies with  
481 viewing and solar geometry. If we again assume 10 independent samples in this geometric  
482 space, then this uncertainty in the overall flux comparison is reduced to  $\pm 1.3\%$ , giving a  
483 total uncertainty in the CERES fluxes for the overall comparison of  $\pm 2.5\%$ .

#### 4.6. Summary of Uncertainties

484 The uncertainties discussed above are summarized in Table 1. When combined, they  
485 indicate that we should expect, with 95% confidence, that the relative difference between  
486 the CERES observations and the modelled reflectance ( $[\text{CERES} - \text{model}]/\text{model}$ ) should  
487 be  $1.9\% \pm 3.7\%$  for radiances and  $1.9\% \pm 3.6\%$  for fluxes. However, the mean difference  
488 in our comparison of measured and modelled radiances is  $-5.2\%$  (median is  $-4.7\%$ ), and  
489 the mean difference in our flux comparison is  $-5.0\%$  (median is  $-5.2\%$ ), both of which  
490 are well outside our expected range. This result differs from that presented by *Dong et al.*  
491 [2008], who found that modelled and observed TOA albedos of deep convective clouds  
492 differ by  $-1\%$  (0.007 of the average albedo of 0.71), with a 95% confidence interval of  
493  $\pm 5\%$ .

494 We have in this section tried to thoroughly evaluate the known potential errors  
495 associated with the modelling, and they are unable to explain the differences we are finding  
496 between the observations and the model. This suggests that either the CERES shortwave  
497 instruments have a negative calibration bias (at least over surfaces that are highly reflective  
498 at short solar wavelengths) or that our model is missing a source of absorption in the  
499 Antarctic atmosphere-snow system. We cannot say conclusively from this study which  
500 of these, or what combination of these, is the answer, but given that CERES is our best  
501 monitoring system of Earth's radiation budget, and that SBDART seems to compare  
502 reasonably well with today's other atmospheric radiative transfer models, it is certainly  
503 an important discrepancy.

## 5. Summary

504 By using a parameterization of the surface reflectance of the East Antarctic Plateau,  
505 based on a set of detailed measurements made there, as the lower boundary in an atmo-  
506 spheric radiative transfer model, we have eliminated what we believe to be the largest  
507 source of uncertainty in modelling solar radiative transfer over the region: modelling the  
508 snow-surface reflectance. The modelled reflectance at the TOA is around 7% less than  
509 the CERES observations, after accounting for known biases in the model. A detailed  
510 uncertainty analysis suggests (with over 99% confidence) that the two values should be  
511 within 5.6% of each other, indicating there is a source of uncertainty that has not been  
512 properly accounted for.

513 We cannot say with certainty whether the unexpected difference between the obser-  
514 vations and the model are a result of modelling error, observation error, or a combination  
515 of the two. Regardless, it is a discrepancy that must be investigated further since both

516 CERES and SBDART (and models similar to it) are widely used. The modelled re-  
517 flectances show better agreement with another satellite instrument (MISR), with a mean  
518 difference of the opposite sign, so this suggests that a solution to the discrepancy should  
519 be sought in the CERES calibration as well as in the model.

520 The East Antarctic Plateau was a useful place to perform this comparison since the  
521 clean, thin, dry atmosphere makes the atmospheric modelling less uncertain, and since  
522 the spatially and temporally homogeneous surface reduces the problems associated with  
523 temporal variability and with spatial matching of the satellite observations and ground  
524 comparison point. However, it is an extreme case in terms of the total flux and the spectral  
525 distribution of flux leaving the top of the atmosphere. It is therefore possible that the  
526 unidentified source of uncertainty has a smaller effect over other darker, or spectrally  
527 different regions.

### 528 **Acknowledgments.**

529 We thank Richard Brandt, Bruce Wielicki, Norman Loeb, Tom Charlock, and  
530 Zhonghai Jin for useful discussions. David Longenecker provided the NOAA ESRL radi-  
531 ation data from South Pole that was used in Section 4.1.3. CERES and MISR data were  
532 obtained from the Atmospheric Science Data Center at the NASA Langley Research Cen-  
533 ter. This research was supported by National Science Foundation grants OPP-00-03826  
534 and ANT-06-36993. Hudson also received funding from the Norwegian Research Council  
535 through the IPY project iAOOS-Norway.

## References

- 536 Aoki, Teruo, Tadao Aoki, M. Fukabori, A. Hachikubo, Y. Tachibana, and F. Nishio (2000),  
537 Effects of snow physical parameters on spectral albedo and bidirectional reflectance of  
538 snow surface, *J. Geophys. Res.*, *105*(D8), 10,219–10,236, doi:10.1029/1999JD901122.
- 539 Brandt, R. E., and S. G. Warren (2009), East Antarctic snow albedo and grain size from  
540 the plateau to the coast, and implications for planetary albedo, *J. Glaciol.*, *submitted*.
- 541 Bruegge, C. J., N. L. Chrien, R. R. Ando, D. J. Diner, W. A. Abdou, M. C. Helmlinger,  
542 S. H. Pilorz, and K. J. Thome (2002), Early validation of the Multi-angle Imaging Spec-  
543 troRadiometer (MISR) radiometric scale, *IEEE Trans. Geosci. Remote Sens.*, *40*(7),  
544 1477–1492, doi:10.1109/TGRS.2002.801583.
- 545 Burrows, J. P., et al. (1999), The Global Ozone Monitoring Experiment (GOME): Mis-  
546 sion concept and first scientific results, *J. Atmos. Sci.*, *56*(2), 151–175, doi:10.1175/  
547 1520-0469(1999)056<0151:TGOMEG>2.0.CO;2.
- 548 Diner, D. J., et al. (1998), Multi-angle Imaging SpectroRadiometer (MISR) instrument  
549 description and experiment overview, *IEEE Trans. Geosci. Remote Sens.*, *36*(4), 1072–  
550 1087, doi:10.1109/36.700992.
- 551 Dong, X., et al. (2008), Using observations of deep convective systems to constrain at-  
552 mospheric column absorption of solar radiation in the optically thick limit, *J. Geophys.*  
553 *Res.*, *113*, D10206, doi:10.1029/2007JD009769.
- 554 Fröhlich, C. (2006), Solar irradiance variability since 1978: Revision of the PMOD  
555 composite during solar cycle 21, *Space Science Reviews*, *125*, 53–65, doi:10.1007/  
556 s11214-006-9046-5.

- 557 Grenfell, T. C., S. G. Warren, and P. C. Mullen (1994), Reflection of solar radiation  
558 by the Antarctic snow surface at ultraviolet, visible, and near-infrared wavelengths, *J.*  
559 *Geophys. Res.*, *99*(D9), 18,669–18,684, doi:10.1029/94JD01484.
- 560 Halthore, R. N., et al. (2005), Intercomparison of shortwave radiative transfer codes and  
561 measurements, *J. Geophys. Res.*, *110*, D11206, doi:10.1029/2004JD005293.
- 562 Hansen, J. E. (1969), Exact and approximate solutions for multiple scattering by  
563 cloudy and hazy planetary atmospheres, *J. Atmos. Sci.*, *26*(3), 478–487, doi:10.1175/  
564 1520-0469(1969)026<0478:EAASFM>2.0.CO;2.
- 565 Hudson, S. R., and S. G. Warren (2007), An explanation for the effect of clouds over  
566 snow on the top-of-atmosphere bidirectional reflectance, *J. Geophys. Res.*, *112*(D19),  
567 D19202, doi:10.1029/2007JD008541.
- 568 Hudson, S. R., S. G. Warren, R. E. Brandt, T. C. Grenfell, and D. Six (2006), Spectral  
569 bidirectional reflectance of Antarctic snow: Measurements and parameterization, *J.*  
570 *Geophys. Res.*, *111*(D18), D18106, doi:10.1029/2006JD007290.
- 571 Hudson, S. R., S. Kato, and S. G. Warren (2009), Evaluating CERES angular distribution  
572 models for snow using surface reflectance observations from the East Antarctic Plateau,  
573 *J. Geophys. Res.*, *submitted*.
- 574 Kato, S., and N. G. Loeb (2005), Top-of-atmosphere shortwave broadband observed radi-  
575 ance and estimated irradiance over polar regions from Clouds and the Earth’s Radiant  
576 Energy System (CERES) instruments on Terra, *J. Geophys. Res.*, *110*, D07202, doi:  
577 10.1029/2004JD005308.
- 578 Kuhn, M., L. S. Kundla, and L. A. Stroschein (1977), The radiation budget at Plateau  
579 Station, Antarctica, 1966-1967, in *Meteorological Studies at Plateau Station, Antarctica*,

- 580 edited by J. A. Businger, pp. 41–73, American Geophysical Union.
- 581 Loeb, N. G. (1997), In-flight calibration of NOAA AVHRR visible and near-IR  
582 bands over Greenland and Antarctica, *Int. J. Remote Sens.*, *18*(3), 477–490, doi:  
583 10.1080/014311697218908.
- 584 Loeb, N. G., K. J. Priestley, D. P. Kratz, E. B. Geier, R. N. Green, B. A. Wielicki,  
585 P. O’Rawe Hinton, and S. K. Nolan (2001), Determination of unfiltered radiances from  
586 the clouds and the earth’s radiant energy system instrument, *J. Appl. Meteorol.*, *40*,  
587 822–835, doi:10.1175/1520-0450(2001)040<0822:DOURFT>2.0.CO;2.
- 588 Masonis, S. J., and S. G. Warren (2001), Gain of the AVHRR visible channel as tracked  
589 using bidirectional reflectance of Antarctic and Greenland snow, *Int. J. Remote Sens.*,  
590 *22*(8), 1495–1520, doi:10.1080/01431160121039.
- 591 Matthews, G., K. Priestley, P. Spence, D. Cooper, and D. Walikainen (2005), Compensa-  
592 tion for spectral darkening of short wave optics occurring on the cloud’s and the Earth’s  
593 radiant energy system, in *Earth Observing Systems X, Proc. SPIE*, vol. 5882, p. 588212,  
594 doi:10.1117/12.618972.
- 595 McClatchey, R. A., R. W. Fenn, J. E. A. Selby, F. E. Volz, and J. S. Garing (1972), *Op-*  
596 *tical Properties of the Atmosphere (Third Edition)*, no. 411 in Environmental Research  
597 Papers, Air Force Cambridge Research Laboratories, Bedford, Massachusetts.
- 598 MISR Science Team (2004), MISR level 1 products quality statement, [http://eosweb.](http://eosweb.larc.nasa.gov/PRODOCS/misr/Quality_Summaries/L1_Products_20040310.html)  
599 [larc.nasa.gov/PRODOCS/misr/Quality\\_Summaries/L1\\_Products\\_20040310.html](http://eosweb.larc.nasa.gov/PRODOCS/misr/Quality_Summaries/L1_Products_20040310.html).
- 600 Pirazzini, R. (2004), Surface albedo measurements over Antarctic sites in summer, *J.*  
601 *Geophys. Res.*, *109*, D20118, doi:10.1029/2004JD004617.

- 602 Rottman, G. (2005), The SORCE mission, *Solar Physics*, *230*, 7–25, doi:10.1007/  
603 s11207-005-8112-6.
- 604 Warren, S. G. (1984), Optical constants of ice from the ultraviolet to the microwave, *Appl.*  
605 *Opt.*, *23*(8), 1206–1225.
- 606 Warren, S. G., and R. E. Brandt (2008), Optical constants of ice from the ultraviolet  
607 to the microwave: A revised compilation, *J. Geophys. Res.*, *113*, D14220, doi:  
608 10.1029/2007JD009744.
- 609 Warren, S. G., R. E. Brandt, and P. O’Rawe Hinton (1998), Effect of surface roughness on  
610 bidirectional reflectance of Antarctic snow, *J. Geophys. Res.*, *103*(E11), 25,789–25,807,  
611 doi:10.1029/98JE01898.
- 612 Warren, S. G., R. E. Brandt, and T. C. Grenfell (2006), Visible and near-ultraviolet  
613 absorption spectrum of ice from transmission of solar radiation into snow, *Appl. Opt.*,  
614 *45*(21), 5320–5334, doi:10.1364/AO.45.005320.

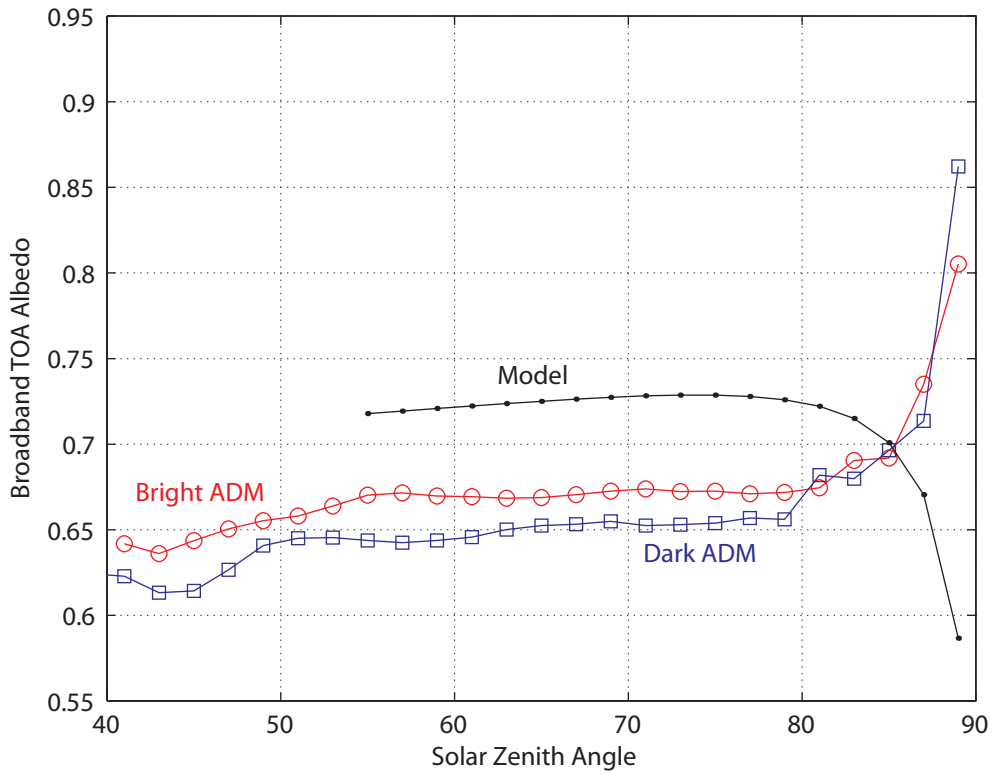


**Figure 1.** A comparison of broadband albedos, versus solar zenith angle, at the TOA from the CERES operational permanent-snow ADMs and from our model.

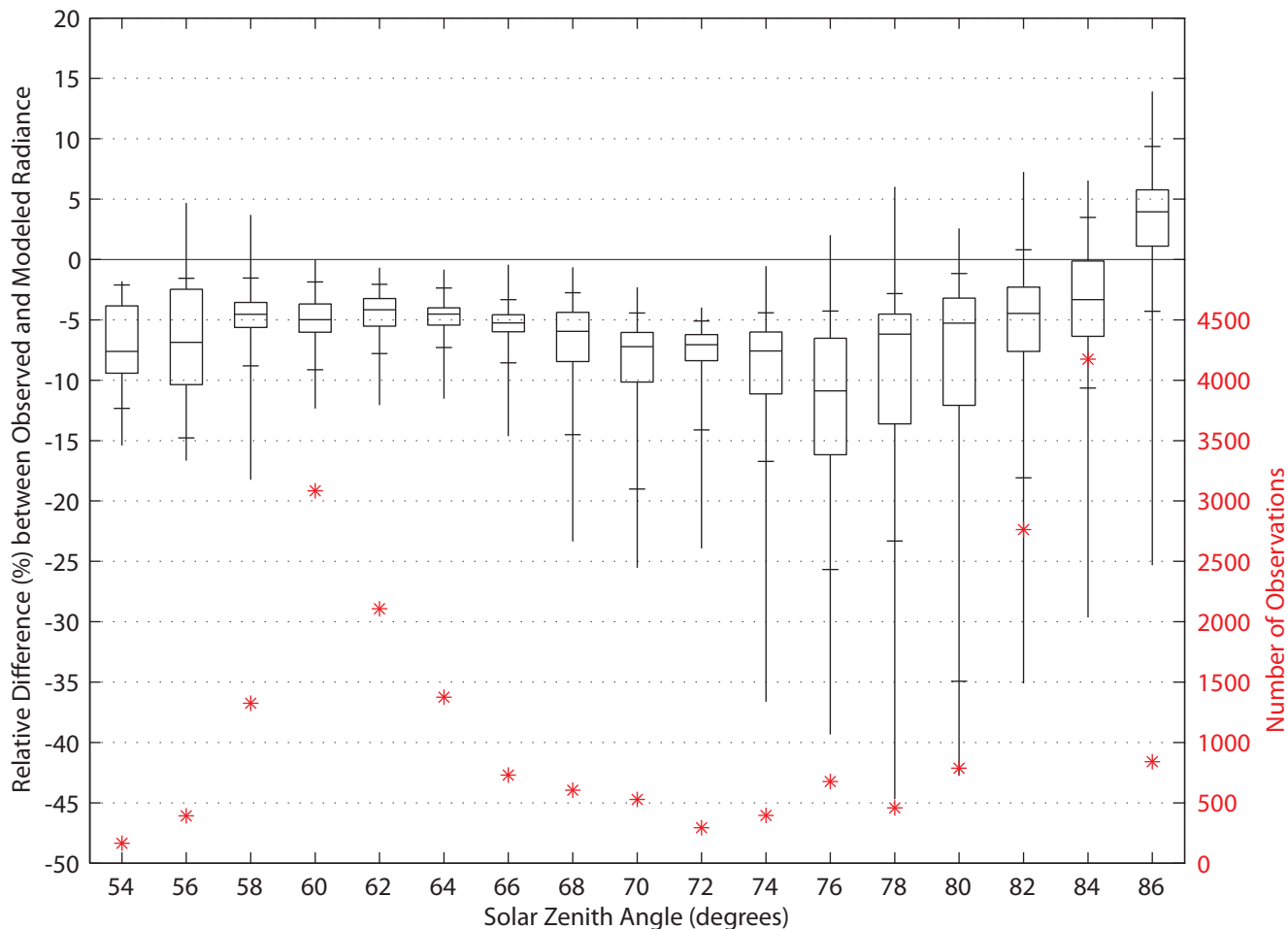


**Figure 2.** The box plots show the relative difference between the CERES-observed and the modelled radiance [ $100 \times (\text{CERES} - \text{model})/\text{model}$ ] within 200 km of Dome C, as a function of solar zenith angle; the boxes extend from the 25<sup>th</sup> to the 75<sup>th</sup> percentiles of the differences, with a horizontal line at the median; the vertical lines extend to the minimum and maximum differences, with horizontal ticks at the 5<sup>th</sup> and 95<sup>th</sup> percentiles. The number of observations used to create each box plot is shown by the red asterisks, referred to the right-hand axis.

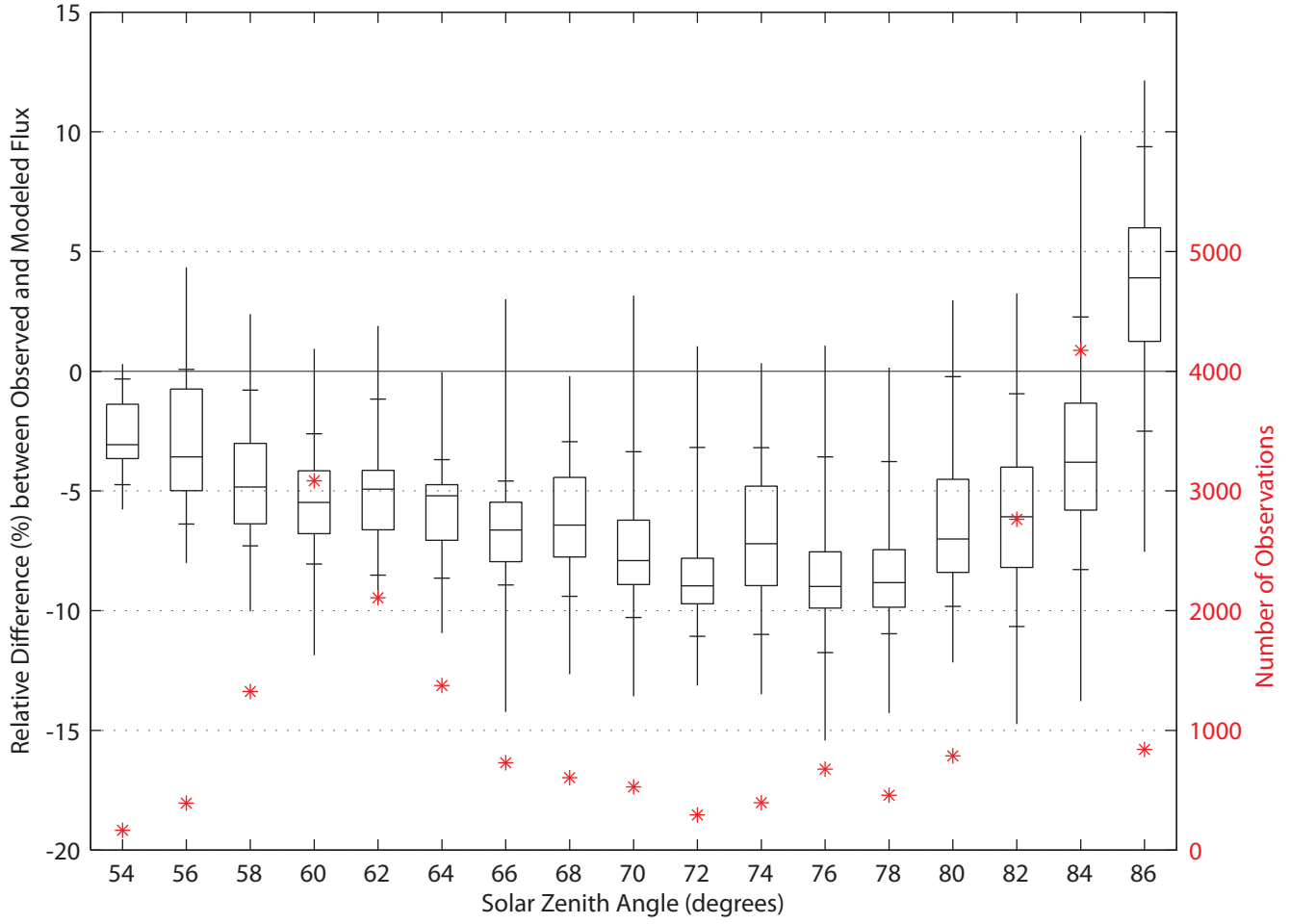


Figure 3. As in Figure 2, but for fluxes instead of radiances.

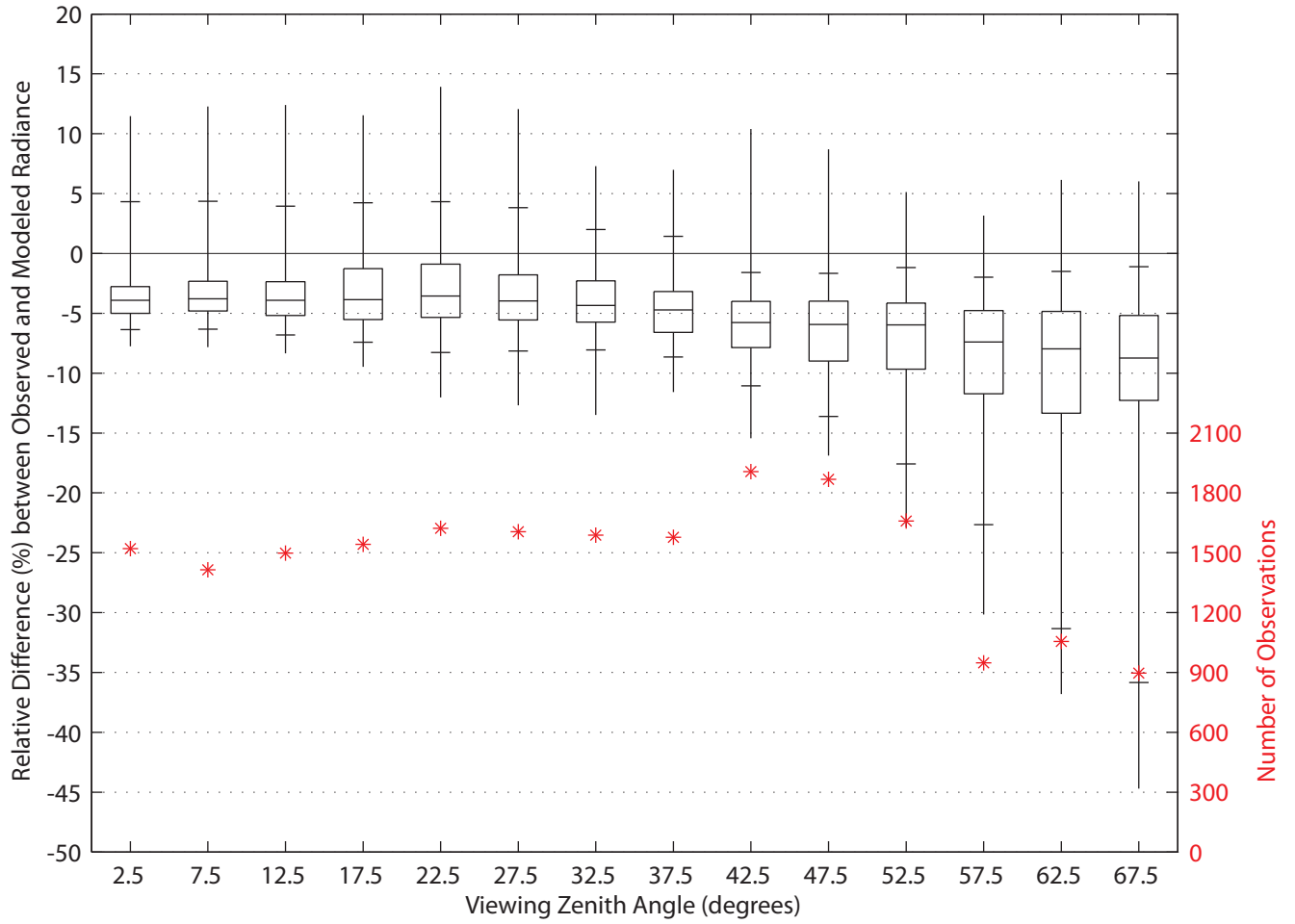


Figure 4. As in Figure 2, but as a function of viewing zenith angle.

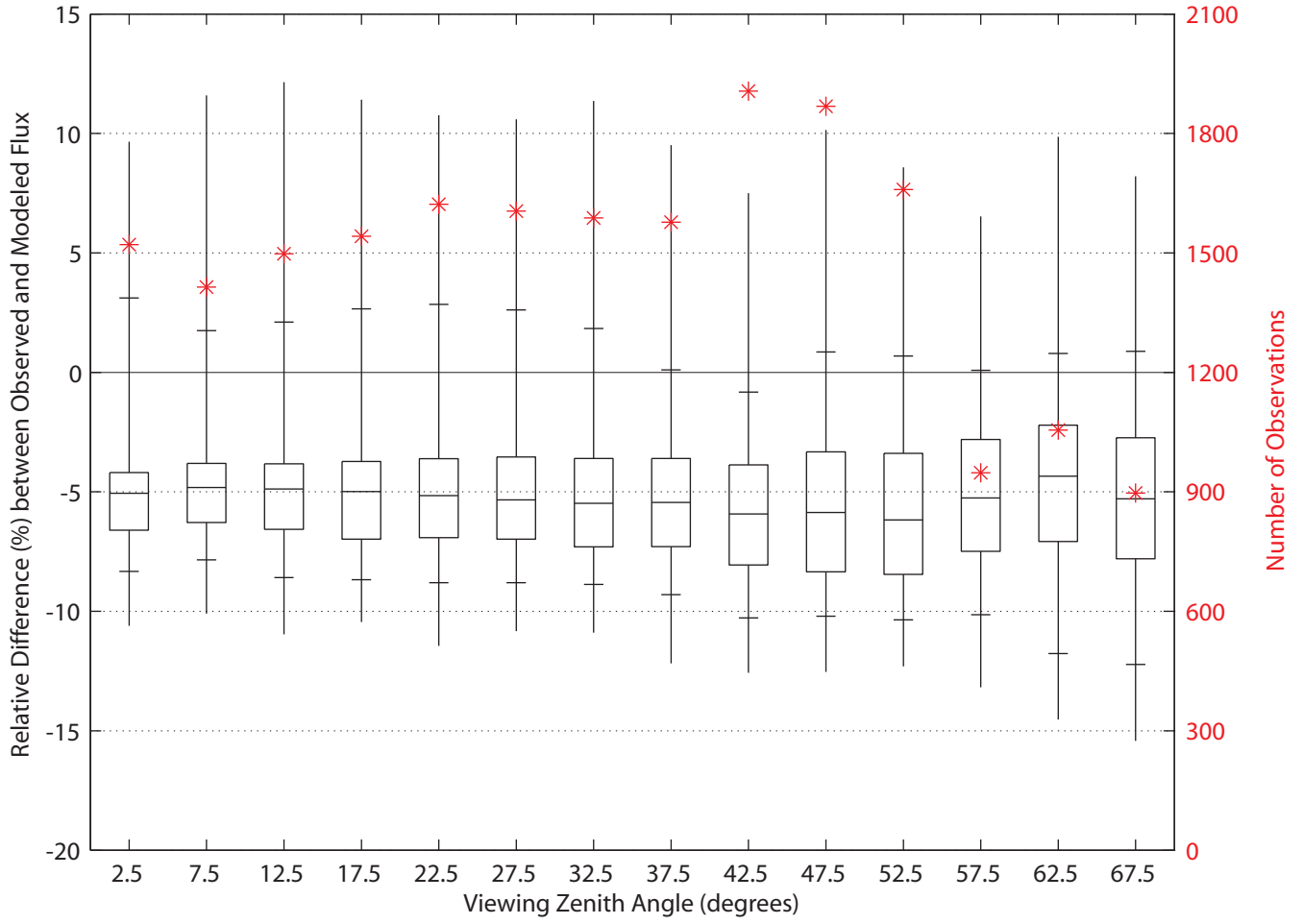
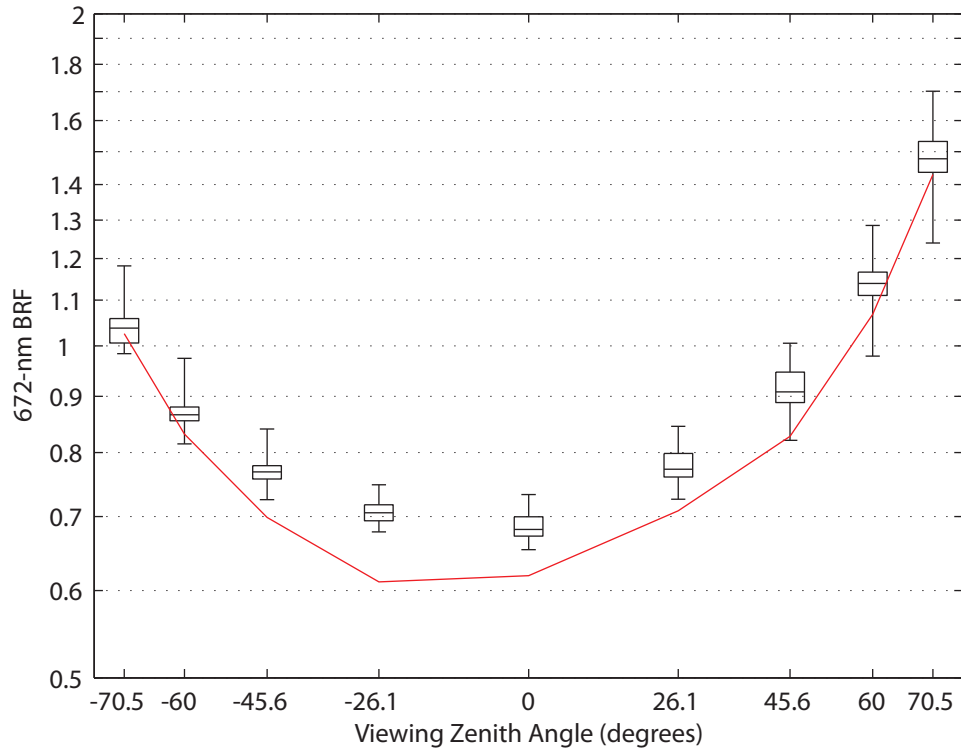


Figure 5. As in Figure 3, but as a function of viewing zenith angle.



**Figure 6.** The box plots show MISR red-channel BRF observations from within 50 km of Dome C during one overpass, at 00:07 local standard time 22 January 2004 (16:07 UTC 21 January 2004); they show the median, upper and lower quartiles, and the range. The modelled BRF for the same solar zenith angle ( $85^\circ$ ) and relative azimuth angles (approximately  $30^\circ$  for  $\theta_v > 0$ ,  $150^\circ$  for  $\theta_v < 0$ ) is shown in red.

**Table 1.** A summary of the uncertainties involved in the comparison between the CERES observations and our model. Some uncertainties or errors have a known sign, but the rest are biases or random uncertainties of unknown sign. The uncertainties for radiance and flux comparisons are listed separately since some apply to only one or the other. All number are in %, and when signed, a positive number indicates something that leads to  $(\text{CERES} - \text{model})/\text{model} > 0$ .

Source	Radiance		Flux	
	known sign	unknown sign	known sign	unknown sign
Modelled surface albedo	-0.8	$\pm 1.2$	-0.8	$\pm 1.2$
Albedo variability	—	$\pm 1.3$	—	$\pm 1.3$
$R$ parameterization	—	$\pm 1.4$	—	—
Gaseous absorption	—	$\pm 1.3$	—	$\pm 1.3$
Atmospheric variability	—	$\pm 0.9$	—	$\pm 0.9$
Incident TOA broadband flux	+2.7	$\pm 0.2$	+2.7	$\pm 0.2$
Solar spectral distribution	—	$\pm 1.0$	—	$\pm 1.0$
CERES data and processing	—	$\pm 2.2$	—	$\pm 2.5$
Total	+1.9	$\pm 3.7$	+1.9	$\pm 3.6$